Journal of Biomechanics 94 (2019) 59–66

Contents lists available at ScienceDirect

Journal of Biomechanics

journal homepage: www.elsevier.com/locate/jbiomech
www.JBiomech.com

Microstructure, mineral and mechanical properties of teleost intermuscular bones

I.A.K. Fiedler [a,b], S. Zeveleva [a], A. Duarte [a], X. Zhao [c], B. Depalle [d], L. Cardoso [e], S. Jin [c], J.P. Berteau [a,f,g,*]

[a] Department of Physical Therapy, City University of New York - College of Staten Island, USA
[b] Department of Osteology and Biomechanics, University Medical Center Hamburg Eppendorf, DE, Germany
[c] Department of Chemistry, City University of New York – College of Staten Island, USA
[d] Department of Materials, Imperial College London, UK
[e] Department of Biomedical Engineering, City University of New York – City College of New York, USA
[f] New York Center for Biomedical Engineering, City University of New York – City College of New York, USA
[g] Nanoscience Initiative, Advanced Science Research Center, City University of New York, USA

ARTICLE INFO

Article history:
Accepted 9 July 2019

Keywords:
Teleost fish
Intermuscular bone
TMD
Mineral
Mechanical properties

ABSTRACT

There is an increasing interest in understanding teleost bone biomechanics in several scientific communities, for instance as interesting biomaterials with specific structure-function relationships. Intermuscular bones of teleost fish have previously been described to play a role in the mechanical force transmission between muscle and bone, but their biomechanical properties are not yet fully described. Here, we have investigated intermuscular bones (IBs) of the *North Atlantic Herring* with regard to their structure and micro-architecture, mineral-related properties, and micro-mechanical tensile properties. A total of 115 IBs from 18 fish were investigated. One cohort of IBs, containing 20 bones from 2 smaller fish and 23 bones of 3 larger fish, was used for mechanical testing, wide-angle X-ray scattering, and scanning electron microscopy. Another cohort, containing 36 bones from 7 smaller fish and 36 bones from 6 larger fish, was used for microCT. Results show some astonishing properties of the IBs: (i) IBs present higher ductility, lower Young's modulus but similar strength and TMD (Tissue Mineral Density) compared to mammalian bone, and (ii) IBs from small fish were 49% higher in Young's modulus than fish bones from larger fish while their TMD was not statistically different and crystal length was 8% higher in large fish bones. Our results revealed that teleost IB presents a hybrid nature of soft and hard tissue that differs from other bone types, which might be associated with their evolution from mineralized tendons. This study provides new data regarding teleost fish bone biomechanical and micro-structural properties.

1. Introduction

Bone is a composite, porous and hierarchized biomaterial consisting of a soft organic matrix of collagen I fibrils, an inorganic hard phase of carbonated hydroxyapatite mineral crystals (cAp), several non-collagenous proteins, and water (Reznikov et al., 2014; Rho et al., 1998). To address the relationship between mineral-related parameters and bone mechanics at different levels of hierarchy, a substantial body of evidence has depicted that poorly mineralized bone presents a weak and ductile behavior, and highly mineralized bone presents a strong and stiff behavior (Burstein et al., 1975; Currey, 1969, 1988; Currey et al., 1996; Martin and Ishida, 1989). For instance, tissue mineral density (TMD) correlated with bending stiffness and failure moment at the whole bone level (Donnelly et al., 2010b), degree of mineralization and crystallinity correlated with stiffness at the tissue level (Wen et al., 2015), and mineral density and cAp thickness correlated with toughness, strength and stiffness at the fibril level (Depalle et al., 2016; Nair et al., 2014; Qin et al., 2012).

Whereas most of the mineral-related and mechanical properties were gained from mammalians, there is increasing interest in other vertebrates like teleost fish (*i.e.* bony fish). For instance, small fish like zebrafish are investigated for studying development and genetic diseases affecting the musculoskeletal system (Fiedler et al., 2018; Laizé et al., 2014; Spoorendonk et al., 2010), and larger fish like salmon, tilapia or swordfish are used for inspiring biomaterials design (Liu and Sun, 2015; Shi et al., 2018) and studying

* Corresponding author at: Department of Physical Therapy, School of Health Sciences at the College of Staten Island, 2800 Victory Boulevard, Staten Island, New York 10314, NY, USA.
E-mail address: Jean.Berteau@csi.cuny.edu (J.P. Berteau).

https://doi.org/10.1016/j.jbiomech.2019.07.009
0021-9290/

structure-function relationships (Atkins et al., 2015; Horton and Summers, 2009; Schmidt et al., 2019; Shahar and Dean, 2013).

One specific type of teleost bone, intermuscular bone (IB), grows within the muscles and originates from tendons (Yao et al., 2015). In previous *ex vivo* investigations of IB, interesting features including a simple structural hierarchy compared to mammalian cortical bone and well-aligned collagen fiber and crystal orientation along the whole bone were described (Burger et al., 2008; Lee and Glimcher, 1991; Rho et al., 2001). One major advantage about testing the mechanical properties of these bones at the whole bone level, is that their structure can be assumed to be more homogeneous and transversely isotropic, than whole bones of *e.g.* mammalians which consist of compact bone, trabecular bone, and an extensive network of vascular channels.

Here, we used the *North Atlantic Herring* to investigate the biomechanical properties of IBs. We hypothesized that IBs (i) show a lower TMD than cortical mammalian bone due to their origin from mineralized tendons, (ii) a higher crystal size and degree of mineralization in bones from large herring fish compared to bones from small fish due to a higher stage of bone growth (*i.e.* larger bone size), and (iii) show a weaker and more ductile mechanical behavior in smaller fish compared to larger fish due to lower mineralization. To test our hypotheses, structure and micro-architecture, mineral-related properties, and micro-mechanical tensile properties of IBs of fish from two groups with different body size were investigated.

2. Material and methods

2.1. Animal model and specimens

A total of 115 IBs from 18 fresh *Atlantic Herring* fish (from a local fish market) were used in this study. As wild-caught fish show natural variations in body measures, IBs were divided into the two groups "small fish" and "large fish" according to their body length (Fig. 1). One IB cohort, containing 43 specimens from 5 fish (20 IBs from "small fish" [body length: 20 and 21 cm; 9 and 11 bones, respectively]), and 23 IBs from three "large fish" [body length: 27, 28 and 28 cm; 6, 9 and 8 bones, respectively) was used for mechanical tensile testing, SEM and WAXS. The mid-shaft part was the region of interest (ROI) for all experiments. The dimensions of the specimens were measured with a micro-caliper under the microscope. Samples had a rod-like shape and elliptical cross-sectional area (A) which was determined based on its long and short diameter. Another cohort, containing 72 IBs from 13 fish were used for microCT (36 bones from 7 "small fish" [body length: 21 ± 1 cm, with 8, 6, 6, 6, 6, 6 and 2 bones per fish], and 36 bones from 6 "large fish" [body length: 26 ± 1 cm, with 6 bones per fish]). Each IB was wrapped in gauze soaked with phosphate buffered saline (PBS) and protease inhibitors, and stored at −20 °C until further processing.

2.2. Micro-mechanical tensile testing

43 IBs (20 from "small fish", 23 from "large fish") were tested using a micro-tensile tester (Xpert4000, ADMET, USA). IBs were positioned vertically inside the grips (customized with serrated pinching grips covered with carbide sand paper to prevent samples from slipping) and their straight, non-curved shafts were aligned with a reference line behind the fixtures (initial gauge length l_0 = 3.0 mm; approximately 3.5 mm of both extremities clamped), s. Suppl. Fig. 1. Samples were kept hydrated during the tests with drops of PBS. Uniaxial loading (quasi-static speed at 10 μm/s (Wright and Hayes, 1976)) was applied while force was measured (100 N load cell). Displacements were recorded as change in actuator position Δl. Conversions from force (F) and displacement (l) to engineering stress (σ) and engineering strain (ε) according to Hooke's law were performed with a custom-written Matlab script (MATLAB 2016b, Mathworks, MA, USA), s. Eqs. (1) and (2)

$$\sigma = F/A \quad (1)$$

$$\varepsilon = \Delta l/l_0 \quad (2)$$

Mechanical parameters were derived as described previously (Depalle et al., 2016; Depalle et al., 2018; Herbert et al., 2016) (Fig. 2A). Reproducibility and accuracy of the set-up and Matlab script were tested on specimens of other materials with similar diameters as the IBs (wood rods, n = 5; polystyrene rods, n = 4; nylon threads, n = 4).

2.3. Scanning electron microscopy (SEM)

SEM imaging (Helios NanoLab, DualBeam, FEI, USA) in low energy secondary electron mode (2 kV, 25 pA) was performed to examine fracture surfaces of a subset of 6 IBs (N = 3/group). Samples were placed upon SEM stubs using carbon tape which was sufficient to increase the conductivity of the specimens' surface.

2.4. Wide-angle X-ray scattering

Eight IBs ("small fish": n = 3, "large fish": n = 5) were investigated using laboratory WAXS (NanoSTAR, Bruker AXS, USA) with a CuKα X-ray source (λ: 0.154 nm, beam size: ~1 mm, acquisition time: 6 h). 2D WAXS patterns were processed using the Scherrer equation (1) with a shape factor of K = 0.9, L (crystal length), λ (X-ray wavelength), B (full width at half maximum in radians),

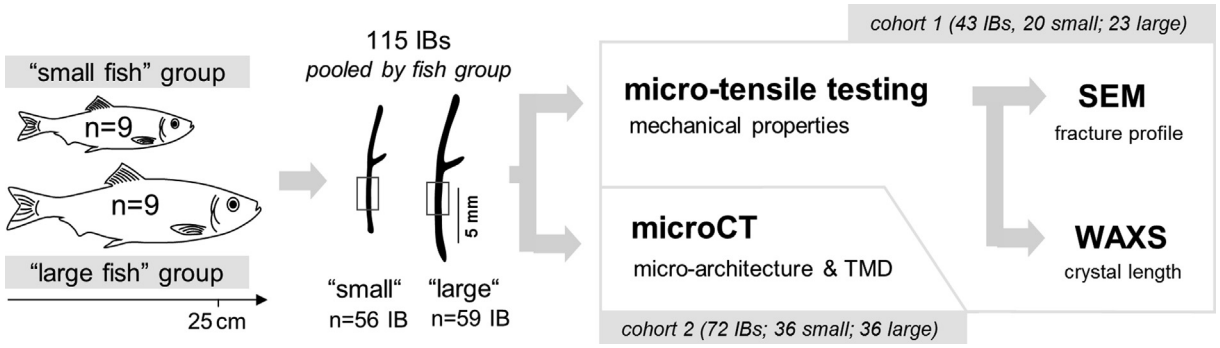

Fig. 1. Experimental set-up of multimodal analysis. A total of 18 herring fish were divided into two groups according to their body length (small" vs. large"). A total of 115 IB specimens were extracted and grouped accordingly. A first cohort was analyzed using micromechanical tensile testing, SEM and WAXS, and a second cohort was investigated using microCT.

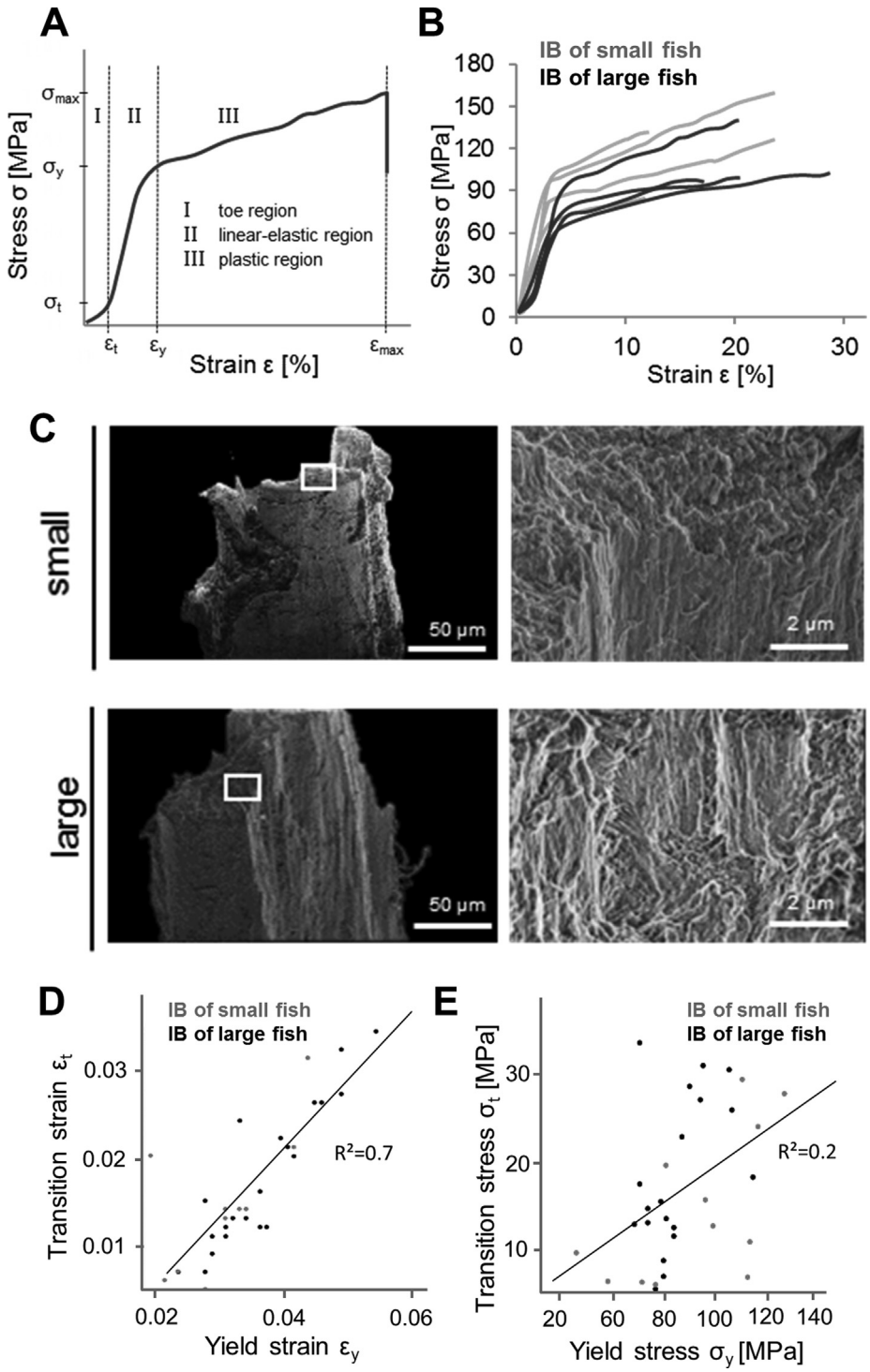

Fig. 2. Mechanical characteristics of intermuscular bone. (A) Exemplary engineering stress-strain curve of IB tested in tension, showing a toe region I from the beginning of the curve until reaching a transition point (σ_t, ε_t), a linear-elastic region II until reaching the yield point (σ_y, ε_y) and a plastic region III until reaching a failure point (σ_{max}, ε_{max}). (B) Engineering stress-strain curves of representative samples from the two fish size groups, where bones from small fish showed significantly higher Young's modulus than bones from large fish. The total amount of strain experienced in the toe region was similar to the amount of strain in the linear-elastic region, contributing 8% and 10% to the total maximum strain, respectively. The strain IBs experienced in region III contributed to the total strain by more than 80%, indicating that IBs have a large capacity for plastic deformation before they undergo failure, yet they show a distinct fracture. (C) SEM micrographs of mechanically tested IB from small and large fish. Both groups display signs of evident transversal fractures, as well as ruptured, fibrous structures and fiber delamination at high magnification. (D) Significant correlations were found between the transition strain and yield strain (Pearson correlation, $R^2 = 0.7$, $p < 0.001$), and (E) between transition stress and yield stress (Pearson correlation, $R^2 = 0.2$, $p = 0.014$) showing that deformations in these two regions are proportional.

and Θ (half of the respective diffraction angle) according to established protocols (Pabisch et al., 2013; Turunen et al., 2016).

$$L = K\lambda/(B\Theta) \quad (3)$$

2.5. High-resolution micro-computed tomography scanning (HR-μCT)

TMD of 72 IBs (n = 36/group) was determined using HR-μCT (SkyScan 1172, Bruker, BE) at 4 μm voxel size, 100 keV and 100 μA. We used a 0.5 mm Aluminum filter for minimizing beam hardening (Fajardo et al., 2009). Image reconstruction and TMD calibration were performed using the software Nrecon (Bruker, BE) (Bouxsein et al., 2010; Palacio-Mancheno et al., 2014). Water and air were scanned with the specimens for conversion of attenuation coefficients to Hounsfield Units (HU) and with hydroxyapatite phantoms (0.25 and 0.75 gHA/cm^3 (smallest commercially available phantoms were ten times larger diameter than the scanned bones) for the conversion from HU to TMD. For a direct comparison to other bone types, additional specimens were scanned under identical imaging conditions: rib bones of Atlantic herring of "small fish" and "large fish" (n = 6/group); and mouse tibiae (n = 2). TMD was assessed over a stack of 300 images for all samples using the software CtAn (Bruker, BE).

2.6. Statistical analysis

Statistical analyses were performed using SPSS (IBM SPSS Statistics, Version 20.0, USA). Normality and homoscedasticity were tested with Shapiro-Wilk's and Levene's tests. Comparisons of mechanical properties were made with independent *t*-test. Comparisons of L were made with the Mann-Whitney-*U* test. Linear relationships were assessed with Pearson. Significance level was α = 0.05.

3. Results

Mechanical characterization showed that IBs of both groups undergo a distinct yield point from a linear-elastic to a plastic region. Furthermore, differences between the two groups for elastic behavior and plastic deformation were found. Mechanical properties and cross-sectional areas are listed in Table 1, and representative stress-strain curves and fracture profiles are shown in Fig. 2B and C. In both groups, profiles presented fracture surfaces indicative of vertical collagen fiber delamination. In some regions, cross-sectional micro-fractures were observed.

With regard to micro-tensile tests, results of performed accuracy and precision measurements on other materials are summarized in Supplemental Table 1 and Supplemental Fig. 2. Mechanical properties were found within the range of literature for wood (Green et al., 1999; Ishimaru et al., 2001; Oloyede and Groombridge, 2000; Sawata and Yasumura, 2003), styrene (Abdellah et al., 2018; George et al., 2000; Rodríguez et al., 2001) and nylon (Chavarria and Paul, 2004; Gyoo et al., 2006; Men et al., 2005). The relative standard uncertainty of measurement of the validated micro-tensile set-up applied on IBs was assessed according to Farrance and Frenkel (2012) and yielded 3.5% and < 0.1% for stress and strain, respectively.

Mechanical properties IB of both groups yielded a significantly (30%) higher Young's modulus in small fish (3.5 (±1.4) GPa) than in large fish (2.6 (±0.5) GPa) (p = 0.005). While yield stress was similar, yield strain was significantly lower in IBs of small fish than IBs of large fish with 0.030 (±0.009) vs. 0.036 (±0.008), p = 0.023. Maximum stress was similar with 110.5 (±23.4) MPa in IBs of small fish and 107.5 (±22.6) MPa in IBs of large fish, and maximum strain was lower in the IBs of small fish with 0.12 (±0.07) compared to the large fish with 0.22 (±0.08), p < 0.001. Total work was smaller in IBs of small fish (10.9 (±8.5) MPa) than in IBs of large fish (19.2 (±8.7) MPa), (p = 0.003), mean plastic work was smaller in IBs of small fish with 10.0 (±8.5) kPa than IBs of large fish with 18.3 (±8.6) kPa (p = 0.003). Elastic work was similar in both groups. No significant differences were measured regarding the transition point from toe to linear-elastic region.

Regarding the transitional behavior of IBs (pooled data of both groups), more than 80% of the specimens (36 out of 43) showed a distinct toe region. On average, the total strain range was composed of 8% strain exhibited within the toe region, 10% strain exhibited within the elastic region, and 82% strain exhibited within the plastic region. Furthermore, Pearson correlations were found between the toe and the elastic region such as between transition and yield strain (p < 0.001 and R^2 = 0.7 [Fig. 2D]), and between transition and yield stress (p < 0.014 and R^2 = 0.2 [Fig. 2E]).

Table 1
Results of the multimodal experimental analysis of intramuscular bone (IB) of Atlantic herring from both fish size groups presented in mean (±standard deviation). Significantly different parameters with a significance level of 0.05 are indicated with an asterisk.

	IB of "small fish"		IB of "large fish"		
	Mechanical properties				
	(n = 20)		(n = 23)		
Transition strain (-)	0.015	(±0.008)	0.018	(±0.008)	
Transition stress (MPa)	14.8	(±9.0)	18.8	(±9.1)	
Yield strain (-)*	0.030	(±0.009)	0.036	(±0.008)	*p = 0.023
Yield stress (MPa)	66.8	(± 23.4)	62.6	(±13.2)	
Young's modulus E (GPa)*	3.5	(±1.4)	2.6	(±0.5)	*p = 0.005
Maximum stress (MPa)	110.5	(±23.4)	107.5	(±22.6)	
Maximum strain (-)	0.12	(±0.07)	0.22	(±0.08)	*p = 0.001
Elastic work (MPa)	0.8	(±0.4)	0.9	(±0.3)	
Plastic work (MPa)	10.0	(±8.5)	18.3	(±8.6)	*p < 0.003
Total work (MPa)	10.9	(±8.5)	19.2	(±8.7)	*p < 0.003
Cross-sectional area (mm^2)*	0.04	(±0.03)	0.09	(±0.02)	*p < 0.001
Transition strain (-)	0.0145	(±0.008)	0.018	(±0.008)	
	Mineral structure				
	(n = 3)		(n = 5)		
Crystal length L (nm)*	12.1	(±0.46)	13.1	(±0.45)	*p = 0.025
	Mineral density				
	(n = 30)		(n = 30)		
TMD (gHAP/cm^3)	1.14	(±0.07)	1.07	(±0.05)	

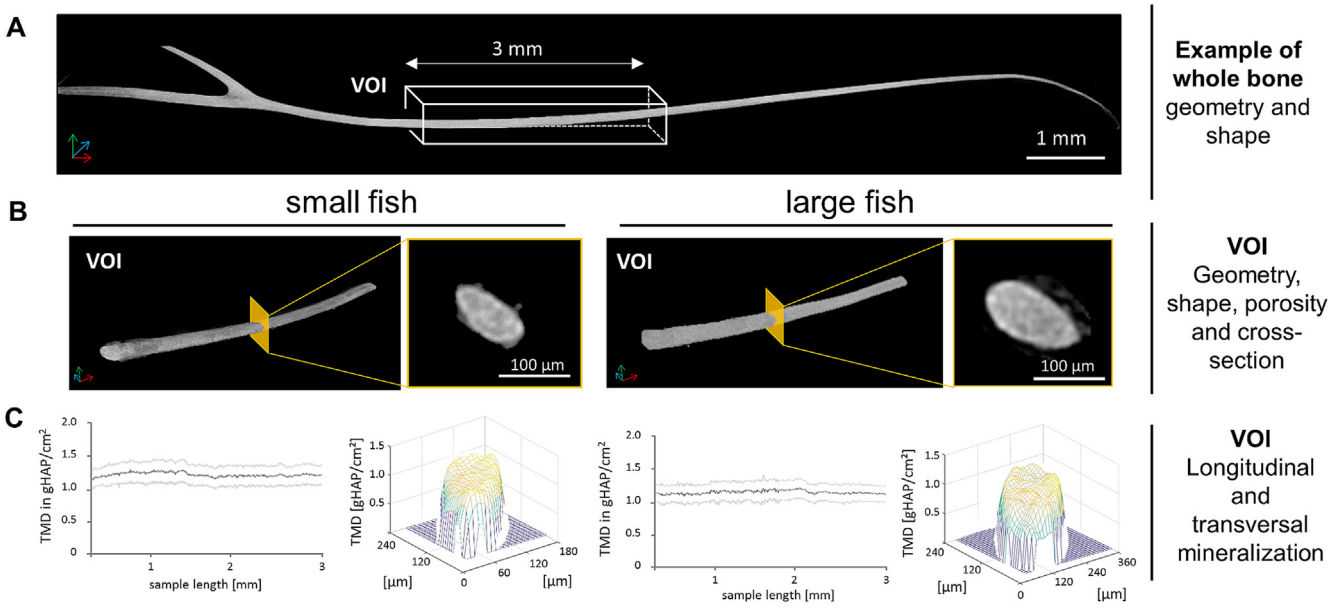

Fig. 3. Microscopic structure and mineral density of intermuscular bones (IBs) assessed with micro-CT at the voxel size of 4 µm. (A) An exemplary 3D reconstruction of a non-tested intermuscular bone with the volume of interest (VOI) investigated within this study. (B) 3D reconstructions of the VOI in IB extracted from small and large fish show a regular, rod-like geometry. Cross-sectional views of IB bone shows ellipsoidal geometry without the presence of porous structures that can be assessed with 4 µm voxel size. (C) Tissue mineral density (TMD) plotted along the long axis of the VOI (left graph, black line corresponds to mean value within a slice, gray lines correspond to the standard deviation within a slice) and TMD plotted across a transversal section. In both size groups and both directions, mineralization appears homogenously distributed, supporting the feasibility of performing tensile testing in the chosen VOI.

An exemplary 3D µCT reconstruction of a whole IB is shown in Fig. 3A. MicroCT imaging at 4 µm voxel size showed that IBs did reveal no porosity at this level of investigation, *i.e.* in the range of 10 µm (Fig. 3B). Fig. 3C, plotting the mean TMD per image slice over the slice number (*i.e.* sample length within VOI), shows a homogeneous TMD distribution along the long axis of the VOI in both groups (*i.e.* horizontal graph with minor noise). Regarding TMD, groups showed similar mean values with 1.14 (±0.07) gHA/cm^3 in IBs of small fish and 1.07 (±0.05) gHA/cm^3 in IBs of large fish. TMD of herring rib bones (1 fish/group, 6 bones each) resulted in 1.08 (±0.23) gHA/cm^3 in small fish and 1.19 (±0.27) gHA/cm^3 in large fish. TMD of mouse tibiae resulted in 1.2 and 1.3 gHA/cm^3. The estimated cAp crystal length L was 12.1 (±0.46) nm for IBs of small fish and 13.1 (±0.45) nm for IBs of large fish with a small but significant difference of 8% ($p = 0.025$, Mann-Whitney *U* test), see Table 1.

4. Discussion

We investigated the Intermuscular Bones (IBs) of *Atlantic Herring* with regard to their structure and micro-architecture, mineral-related properties, and micro-mechanical tensile properties (n = 115 IBs). IBs had a cylindrical, thin, fiber-like geometrical shape with a homogenous ellipsoidal cross-sectional area in their mid-shaft region which served as the VOI within this study. IBs showed mechanical deformation characteristics of soft tissue (*e.g.* tendons, ligaments) and hard tissue (*e.g.* mammalian cortical bone). TMD was independent of fish size, while 8% longer crystals and a 30% lower Young's modulus were displayed in the IBs from large fish.

MicroCT imaging was used to assess TMD and to display the structure and internal micro-architecture of IBs. Imaging of the mid-shaft region showed that IBs had a longitudinally homogeneous mineralization, based on the low variance of both cross-sectional area (pixels within masked image slices) and low variance of TMD values across the image slices (s. Fig. 3). Based on previous publications employing microCT to assess mineral heterogeneity (Lloyd et al., 2015), we suggest that IBs were suitable for whole bone micro-mechanical tensile testing within the VOI and meet the assumptions of Hooke's law. Regarding the micro-architecture of IB, a solid structure with no porosity in the range of 10 µm was found. Although we have shown that a voxel size of 4 µm was sufficient to display vascular porosity in the range of 10 µm in cortical bone of small animals (Palacio-Mancheno et al., 2014; Sharma et al., 2018), microCT images in this study did not reveal such pores or vascular channels. Nanoscopic porosities and lacunar-canalicular structures below 10 µm are likely present in IB but not detectable with the employed microCT acquisition parameters. Because erythrocytes in herring fish have been reported in the range of 10 µm (long diameter) and 6–8 µm (short diameter) (Wilkins and Clarke, 1974; Witeska, 2013), we suggest that vascular channels, if present, are smaller in IB compared to cortical bone of other small animals like mice. To summarize, our results support the assumption of a simpler internal structure in IB (Burger et al., 2008; Glimcher, 1959) than in human whole bones – composed of several hierarchical levels including cortical and trabecular compartments, osteonal structures, and vascular porosity (Reznikov et al., 2014).

Regarding TMD, the percentage difference between IBs of small and large fish (1.14 gHA/cm^3 vs. 1.07 gHA/cm^3) was 6% without reaching significance, which does not support our initial hypotheses of low mineralization in IB compared to mammalian bone and lower mineralization in bones from small compared to large fish. While smaller absolute values in TMD were expected due to the observed soft-tissue-like mechanical deformation characteristics, our results indicate a similar degree of mineralization as commonly reported for fish bones of up to 1 gHA/cm^3 (Cohen et al., 2012) or mouse and human bone (Granke et al., 2015a; Main et al., 2014). However, for delivering local Calcium content and mineral heterogeneity at high-resolution, IBs should be investigated with quantitative back-scattered imaging (Roschger et al.,

2008). This technique would also provide a better understanding of sub-micrometer-sized porosity, which can lead to an underestimation of TMD when assessed at lower resolution, *i.e.* the micrometer scale, as applied in this study.

Using our micro-mechanical tensile testing set-up we showed that IBs show an interesting combination of mechanical characteristics of hard tissues (*e.g.* mammalian cortical bone) and soft tissues (*e.g.* tendon). Specifically, IBs presented hard tissue characteristics including similar strength as mammalian cortical bone (Carter and Spengler, 1978; Cowin, 1983; Li et al., 2013; Mirzaali et al., 2016), while soft tissue characteristics included a Young's modulus of one order of magnitude lower than reported values of mammalian cortical bone, and distinct plastic deformation. IBs fracture strains reached up to 22% which is much higher than mammalian cortical bone which elongates only by a few percents (Liu et al., 2014), or tendons with maximum strains around 10% (Matson et al., 2012). Indeed, 80% of total strain was on average expressed during the plastic deformation regime (region III in the stress-strain curve), and the Young's modulus of IBs was in the magnitude of light, non-mineralized tendons (Bennett et al., 1986; Matson et al., 2012). Based on the presence of these soft- and hard tissue characteristics in the stress-strain curves, our results suggest that IBs have a particular combination of properties which may be governed by its microstructural organization that is derived from tendons within the musculoskeletal system of the teleost (Yao et al., 2015).

Interestingly, more than 80% of all IBs showed a distinct toe region before entering linear elastic deformation, which was not observed in other materials using the identical test protocol (Supplemental Fig. 2). Whereas the presence of such toe regions has previously been explained in terms of uncrimping of collagen fibers in mechanical tensile tests of tendons (Lake et al., 2009) and in simulations of individual mineralized fibers (Depalle et al., 2016), the testing set-up used in this study did not allow for stereo-correlation, *in situ* crystallography, or direct observations of such crimping or uncoiling effects in IB. While a closer investigation of the tendon-like appearance is required, significant linear correlations have been found between the transition point and the yield point. The variance of the transition point strain explained 70% of the variance of the yield strain, while the variance of the transition point stress explained 20% of the variance of the yield stress.

Crystal length was < 15 nm for both groups which is below values reported for mammalian bones (Acerbo et al., 2014) and for herring IBs when assessed with small-angle X-ray scattering (up to 54 nm (Burger et al., 2008)). This discrepancy could be linked to several factors. As we detected a slightly larger crystal length in the bones of larger fish, the observed difference may be associated with a size effect: IBs in Burger et al. (2008) had a diameter of 500 μm. Moreover, acquisitions herein were gained from the mid-shaft region of the IB, whereas Burger et al. investigated in a different region of interest above the spur. Furthermore, the evaluation of crystal length using the Scherrer equation requires the input of a shape factor K which varies from 0.9 to 2 depending on crystal structure and literature (Monshi et al., 2012; Ziv and Weiner, 2009). Here, K of 0.9 was used as the gold standard for carbonated hydroxyapatite in bone tissues. To additionally visualize the crystal phase in IB, transmission electron microscopy of ultra-thin lamellae of one IB sample from large fish (Suppl. Fig. 3) was performed, supporting that IB is built of collagen fibers aligned along the long axis with the typical collagen periodicity and embedded, well-aligned inorganic crystals (~2–4 nm in thickness).

Whereas the sample size for WAXS measurements was much smaller compared to mechanical testing and TMD assessment, we found 8% larger crystals in IB from the "large fish" group compared to the "small fish" group, similar to previously described changes of the crystal phase during bone tissue maturation (Donnelly et al., 2010a; Jäger and Fratzl, 2000; Nair et al., 2013; Vercher-Martinez et al., 2015; Ziv and Weiner, 2009). While such small changes in crystal size alone are unlikely to induce measurable differences in mechanical performance, a lower Young's modulus was detected in large compared to small IBs, not supporting our initial hypothesis. This could be related to degradation of the bone matrix, *e.g.* the suggested lack of remodeling in this tissue might lead to micro-cracks, or nano-porous structures could develop with larger bone size, also bearing a possible explanation for a slightly lower TMD in fish of larger fish size. However, whether assessed differences between IBs from the two groups are related to development, maturation, growth, or advanced aging of the fish cannot be revealed without quantification of the fish age. As several factors including nutrition, environment, and temperature lead to variations in fish from the same chronological age, specifically in wild-caught fish (Talbot, 1993), it is impossible to determine the precise age of the fish based on its body length and we cannot validate whether the detected differences in mechanical properties or in crystal size were influenced by growth or advanced aging of the fish. Additional high-resolution imaging and testing in the scope of a longitudinal study will be required to provide a better understanding of the mechanical and structural features, collagen-mineral interaction, and age-dependent changes of IB.

In conclusion, we present new data on IB with a rare combination of stiffness, strength, and toughness compared to other bone types. An in-depth high-resolution analysis of the composition, porosity, and interconnectivity of the collagen in IBs could help reveal the specific failure mechanisms in this type of mineralized tissue. As porosity is known to affect bone mechanical properties (Bala et al., 2016; Granke et al., 2015b), IB with lower dimensions of porosity compared to mammalian bone may be useful for investigating the relationship between biological components and mechanics of mineralized tissues. While an explanation for the nano-structural and molecular origin of the particular mechanical behavior of IBs is outside the scope of this study, we propose IBs as an interesting tissue to study the complex interplay between a collagenous soft phase and a reinforced hard mineral phase.

Acknowledgments

Work supported by NSF (CMMI-1333560, MRI-1229449), NIH (DK103362) (L.C.), Wellcome Trust WT097347MA (B.D.), PSC CUNY grant 68853-0046 (J.P.B.). Authors thank Guillaume Courtemanche (CUNY-CSI) for technical assistance and Chaim M. Zieg for acquiring fresh Atlantic herring.

Declaration of Competing Interest

Authors declare no conflict of interest.

Appendix A. Supplementary material

Supplementary data to this article can be found online at https://doi.org/10.1016/j.jbiomech.2019.07.009.

References

Abdellah, M., Fathi, H., Abdelhaleem, A., Dewidar, M., 2018. Mechanical properties and wear behavior of a novel composite of acrylonitrile–butadiene–styrene strengthened by short basalt fiber. J. Comp. Sci. 2, 34.

Acerbo, A.S., Kwaczala, A.T., Yang, L., Judex, S., Miller, L.M., 2014. Alterations in collagen and mineral nanostructure observed in osteoporosis and pharmaceutical treatments using simultaneous small- and wide-angle X-ray scattering. Calcif. Tissue Int. 95, 446–456.

Atkins, A., Milgram, J., Weiner, S., Shahar, R., 2015. The response of anosteocytic bone to controlled loading. J. Exp.l Biol. 218, 3559–3569.
Bala, Y., Lefèvre, E., Roux, J.-P., Baron, C., Lasaygues, P., Pithioux, M., Kaftandjian, V., Follet, H., 2016. Pore network microarchitecture influences human cortical bone elasticity during growth and aging. J. Mech. Behav. Biomed. Mater. 63, 164–173.
Bennett, M.B., Ker, R.F., Imery, N.J., Alexander, R.M., 1986. Mechanical properties of various mammalian tendons. J. Zool. 209, 537–548.
Bouxsein, M.L., Boyd, S.K., Christiansen, B.A., Guldberg, R.E., Jepsen, K.J., Müller, R., 2010. Guidelines for assessment of bone microstructure in rodents using micro-computed tomography. J. Bone Miner. Res.: Offic. J. Am. Soc. Bone Miner. Res. 25, 1468–1486.
Burger, C., Zhou, H.-W., Sicŝ, I., Hsiao, B.S., Chu, B., Graham, L., Glimcher, M.J., 2008. Small-angle X-ray scattering study of intramuscular fish bone. Collagen fibril superstructure determined from equidistant meridional reflections. J. Appl. Crystallogr. 41, 252–261.
Burstein, A.H., Zika, J.M., Heiple, K.G., Klein, L., 1975. Contribution of collagen and mineral to the elastic-plastic properties of bone. J. Bone Joint Surg. Am. 57, 956–961.
Carter, D.R., Spengler, D.M., 1978. Mechanical properties and composition of cortical bone. Clin. Orthop. Relat. Res., 192–217
Chavarria, F., Paul, D.R., 2004. Comparison of nanocomposites based on nylon 6 and nylon 66. Polymer 45, 8501–8515.
Cohen, L., Dean, M., Shipov, A., Atkins, A., Monsonego-Ornan, E., Shahar, R., 2012. Comparison of structural, architectural and mechanical aspects of cellular and acellular bone in two teleost fish. J. Exp. Biol. 215, 1983–1993.
Cowin, S.C., 1983. The mechanical and stress adaptive properties of bone. Ann. Biomed. Eng. 11, 263–295.
Currey, J.D., 1969. The relationship between the stiffness and the mineral content of bone. J. Biomech. 2, 477–480.
Currey, J.D., 1988. The effect of porosity and mineral content on the Young's modulus of elasticity of compact bone. J. Biomech. 21, 131–139.
Currey, J.D., Brear, K., Zioupos, P., 1996. The effects of ageing and changes in mineral content in degrading the toughness of human femora. J. Biomech. 29, 257–260.
Depalle, B., Duarte, A.G., Fiedler, I.A.K., Pujo-Menjouet, L., Buehler, M.J., Berteau, J.-P., 2018. The different distribution of enzymatic collagen cross-links found in adult and children bone result in different mechanical behavior of collagen. Bone 110, 107–114.
Depalle, B., Qin, Z., Shefelbine, S.J., Buehler, M.J., 2016. Large deformation mechanisms, plasticity, and failure of an individual collagen fibril with different mineral content. J. Bone Miner. Res. 31, 380–390.
Donnelly, E., Boskey, A.L., Baker, S.P., van der Meulen, M.C.H., 2010a. Effects of tissue age on bone tissue material composition and nanomechanical properties in the rat cortex. J. Biomed. Mater. Res. Part A 92, 1048–1056.
Donnelly, E., Chen, D.X., Boskey, A.L., Baker, S.P., van, M.d.M., 2010b. Contribution of mineral to bone structural behavior and tissue mechanical properties. Calcif. Tissue Int. 87, 450–460.
Fajardo, R.J., Cory, E., Patel, N.D., Nazarian, A., Laib, A., Manoharan, R.K., Schmitz, J.E., DeSilva, J.M., MacLatchy, L.M., Snyder, B.D., Bouxsein, M.L., 2009. Specimen size and porosity can introduce error into microCT-based tissue mineral density measurements. Bone 44, 176–184.
Farrance, I., Frenkel, R., 2012. Uncertainty of measurement. A review of the rules for calculating uncertainty components through functional relationships. Clin. Biochem. Rev. 33, 49–75.
Fiedler, I.A.K., Schmidt, F.N., Wölfel, E.M., Plumeyer, C., Milovanovic, P., Gioia, R., Tonelli, F., Bale, H.A., Jähn, K., Besio, R., Forlino, A., Busse, B., 2018. Severely impaired bone material quality in Chihuahua zebrafish resembles classical dominant human osteogenesis imperfecta. J. Bone Miner. Res.: Offic. J. Am. Soc. Bone Miner. Res. 33, 1489–1499.
George, S.C., Ninan, K.N., Groeninckx, G., Thomas, S., 2000. Styrene-butadiene rubber/natural rubber blends. Morphology, transport behavior, and dynamic mechanical and mechanical properties. J. Appl. Polym. Sci. 78, 1280–1303.
Glimcher, M.J., 1959. Molecular biology of mineralized tissues with particular reference to bone. Rev. Mod. Phys. 31, 359–393.
Granke, M., Does, M.D., Nyman, J.S., 2015a. The role of water compartments in the material properties of cortical bone. Calcif. Tissue Int. 97, 292–307.
Granke, M., Grimal, Q., Parnell, W.J., Raum, K., Gerisch, A., Peyrin, F., Saïed, A., Laugier, P., 2015b. To what extent can cortical bone millimeter-scale elasticity be predicted by a two-phase composite model with variable porosity? Acta Biomater. 12, 207–215.
Green, D.W., Winandy, J.E., Kretschmann, D.E., 1999. Mechanical Properties of Wood. Chapter 4. In: Forest Products Laboratory (Ed.). Wood Handbook - Wood as an Engineering Material. Gen. Tech. Rep. FPL–GTR–113., Madison, WI.
Gyoo, P.M., Venkataramani, S., Kim, S.C., 2006. Morphology, thermal, and mechanical properties of polyamide 66/clay nanocomposites with epoxy-modified organoclay. J. Appl. Polym. Sci. 101, 1711–1722.
Herbert, A., Brown, C., Rooney, P., Kearney, J., Ingham, E., Fisher, J., 2016. Bi-linear mechanical property determination of acellular human patellar tendon grafts for use in anterior cruciate ligament replacement. J. Biomech. 49, 1607–1612.
Horton, J.M., Summers, A.P., 2009. The material properties of acellular bone in a teleost fish. J. Exp. Biol. 212, 1413–1420.
Ishimaru, Y., Arai, K., Mizutani, M., Oshima, K., Iida, I., 2001. Physical and mechanical properties of wood after moisture conditioning. J. Wood Sci. 47, 185–191.
Jäger, I., Fratzl, P., 2000. Mineralized collagen fibrils. A mechanical model with a staggered arrangement of mineral particles. Biophys. J. 79, 1737–1746.
Laizé, V., Gavaia, P.J., Cancela, M.L., 2014. Fish. A suitable system to model human bone disorders and discover drugs with osteogenic or osteotoxic activities.
Lake, S.P., Miller, K.S., Elliott, D.M., Soslowsky, L.J., 2009. Effect of fiber distribution and realignment on the nonlinear and inhomogeneous mechanical properties of human supraspinatus tendon under longitudinal tensile loading. J. Orthop. Res.: Offic. Public. Orthop. Res. Soc. 27, 1596–1602.
Lee, D.D., Glimcher, M.J., 1991. Three-dimensional spatial relationship between the collagen fibrils and the inorganic calcium phosphate crystals of pickerel (Americanus americanus) and herring (Clupea harengus) bone. J. Mol. Biol. 217, 487–501.
Li, S., Demirci, E., Silberschmidt, V.V., 2013. Variability and anisotropy of mechanical behavior of cortical bone in tension and compression. J. Mech. Behav. Biomed. Mater. 21, 109–120.
Liu, C., Sun, J., 2015. Hydrolyzed tilapia fish collagen induces osteogenic differentiation of human periodontal ligament cells. Biomed. Mater. (Bristol, England) 10, 65020.
Liu, Y., Thomopoulos, S., Chen, C., Birman, V., Buehler, M.J., Genin, G.M., 2014. Modelling the mechanics of partially mineralized collagen fibrils, fibres and tissue. J. R. Soc. Interface 11, 20130835.
Lloyd, A.A., Wang, Z.X., Donnelly, E., 2015. Multiscale contribution of bone tissue material property heterogeneity to trabecular bone mechanical behavior. J. Biomech. Eng. 137.
Main, R.P., Lynch, M.E., van der Meulen, M.C.H., 2014. Load-induced changes in bone stiffness and cancellous and cortical bone mass following tibial compression diminish with age in female mice. J. Exp. Biol. 217, 1775–1783.
Martin, R.B., Ishida, J., 1989. The relative effects of collagen fiber orientation, porosity, density, and mineralization on bone strength. J. Biomech. 22, 419–426.
Matson, A., Konow, N., Miller, S., Konow, P.P., Roberts, T.J., 2012. Tendon material properties vary and are interdependent among turkey hindlimb muscles. J. Exp. Biol. 215, 3552–3558.
Men, Y., Rieger, J., Hong, K., 2005. Critical strains in tensile deformed polyamide 6 and 6/66 copolymer. J. Polym. Sci., Part B: Polym. Phys. 43, 87–96.
Mirzaali, M.J., Schwiedrzik, J.J., Thaiwichai, S., Best, J.P., Michler, J., Zysset, P.K., Wolfram, U., 2016. Mechanical properties of cortical bone and their relationships with age, gender, composition and microindentation properties in the elderly. Bone 93, 196–211.
Monshi, A., Foroughi, M.R., Monshi, M.R., 2012. Modified Scherrer equation to estimate more accurately nano-crystallite size using XRD. World J. Nano Sci. Eng. 02, 154–160.
Nair, A.K., Gautieri, A., Buehler, M.J., 2014. Role of intrafibrillar collagen mineralization in defining the compressive properties of nascent bone. Biomacromolecules 15, 2494–2500.
Nair, A.K., Gautieri, A., Chang, S.-W., Buehler, M.J., 2013. Molecular mechanics of mineralized collagen fibrils in bone. Nat. Commun. 4, 1724.
Oloyede, A., Groombridge, P., 2000. The influence of microwave heating on the mechanical properties of wood. J. Mater. Process. Technol. 100, 67–73.
Pabisch, S., Wagermaier, W., Zander, T., Li, C., Fratzl, P., 2013. Imaging the nanostructure of bone and dentin through small- and wide-angle X-ray scattering. Methods Enzymol. 532, 391–413.
Palacio-Mancheno, P.E., Larriera, A.I., Doty, S.B., Cardoso, L., Fritton, S.P., 2014. 3D assessment of cortical bone porosity and tissue mineral density using high-resolution μCT. Effects of resolution and threshold method. J. Bone Miner. Res.: Offic. J. Am. Soc. Bone Miner. Res. 29, 142–150.
Qin, Z., Gautieri, A., Nair, A.K., Inbar, H., Buehler, M.J., 2012. Thickness of hydroxyapatite nanocrystal controls mechanical properties of the collagen-hydroxyapatite interface. Langmuir: ACS J. Surf. Colloids 28, 1982–1992.
Reznikov, N., Shahar, R., Weiner, S., 2014. Bone hierarchical structure in three dimensions. Acta Biomater. 10, 3815–3826.
Rho, J.Y., Mishra, S.R., Chung, K., Bai, J., Pharr, G.M., 2001. Relationship between ultrastructure and the nanoindentation properties of intramuscular herring bones. Ann. Biomed. Eng. 29, 1082–1088.
Rho, J.-Y., Kuhn-Spearing, L., Zioupos, P., 1998. Mechanical properties and the hierarchical structure of bone. Med. Eng. Phys. 20, 92–102.
Rodríguez, J.F., Thomas, J.P., Renaud, J.E., 2001. Mechanical behavior of acrylonitrile butadiene styrene (ABS) fused deposition materials Experimental investigation. Rapid Prototyp. J. 7, 148–158.
Roschger, P., Paschalis, E.P., Fratzl, P., Klaushofer, K., 2008. Bone mineralization density distribution in health and disease. Bone 42, 456–466.
Sawata, K., Yasumura, M., 2003. Estimation of yield and ultimate strengths of bolted timber joints by nonlinear analysis and yield theory. J. Wood Sci. 49, 383–391.
Schmidt, F.N., Zimmermann, E.A., Walsh, F., Plumeyer, C., Schaible, E., Fiedler, I.A.K., Milovanovic, P., Rößle, M., Amling, M., Blanchet, C., Gludovatz, B., Ritchie, R.O., Busse, B., 2019. On the origins of fracture toughness in advanced teleosts. how the swordfish sword's bone structure and composition allow for slashing under water to kill or stun prey. Adv. Sci. 12, 1900287.
Shahar, R., Dean, M.N., 2013. The enigmas of bone without osteocytes. BoneKEy Rep. 2, 343.
Sharma, D., Larriera, A.I., Palacio-Mancheno, P.E., Gatti, V., Fritton, J.C., Bromage, T. G., Cardoso, L., Doty, S.B., Fritton, S.P., 2018. The effects of estrogen deficiency on cortical bone microporosity and mineralization. Bone 110, 1–10.
Shi, P., Liu, M., Fan, F., Yu, C., Lu, W., Du, M., 2018. Characterization of natural hydroxyapatite originated from fish bone and its biocompatibility with osteoblasts. Mater. Sci. Eng. C, Mater. Biol. Applic. 90, 706–712.
Spoorendonk, K.M., Hammond, C.L., Huitema, L.F.A., Vanoevelen, J., Schulte-Merker, S., 2010. Zebrafish as a unique model system in bone research. The power of genetics and in vivo imaging. J. Appl. Ichthyol. 26, 219–224.
Talbot, C., 1993. Some aspects of the biology of feeding and growth in fish. Proc. Nutr. Soc. 52, 403–416.

Turunen, M.J., Kaspersen, J.D., Olsson, U., Guizar-Sicairos, M., Bech, M., Schaff, F., Tagil, M., Jurvelin, J.S., Isaksson, H., 2016. Bone mineral crystal size and organization vary across mature rat bone cortex. J. Struct. Biol. 195, 337–344.
Vercher-Martinez, A., Giner, E., Arango, C., Fuenmayor, F.J., 2015. Influence of the mineral staggering on the elastic properties of the mineralized collagen fibril in lamellar bone. J. Mech. Behav. Biomed. Mater. 42, 243–256.
Wen, X.-X., Wang, F.-Q., Xu, C., Wu, Z.-X., Zhang, Y., Feng, Y.-F., Yan, Y.-B., Lei, W., 2015. Time related changes of mineral and collagen and their roles in cortical bone mechanics of ovariectomized rabbits. PLoS ONE 10, e0127973.
Wilkins, N.P., Clarke, F.L., 1974. The size and shape of erythrocytes in the herring Clupea harengus L. Comp. Biochem. Physiol. A Physiol. 47, 341–345.
Witeska, M., 2013. Erythrocytes in teleost fishes A review. Zool. Ecol. 23, 275–281.
Wright, T.M., Hayes, W.C., 1976. Tensile testing of bone over a wide range of strain rates. Effects of strain rate, microstructure and density. Med. Biol. Eng. 14, 671–680.
Yao, W., Lv, Y., Gong, X., Wu, J., Bao, B., 2015. Different ossification patterns of intermuscular bones in fish with different swimming modes. Biol. Open 4, 1727–1732.
Ziv, V., Weiner, S., 2009. Bone crystal sizes. A comparison of transmission electron microscopic and X-Ray diffraction line width broadening techniques. Connect. Tissue Res. 30, 165–175.